 Letter

Optics Letters

Birefringence compensation method of test-mass substrates for gravitational wave detectors with arbitrary polarization states

MARC EISENMANN,[1,*] SHALIKA SINGH,[1] AND MATTEO LEONARDI[1,2]

[1] National Astronomical Observatory of Japan, 2-21-1 Osawa, Mitaka, Tokyo 181-8588, Japan
[2] Università di Trento, Dipartimento di Fisica, I-38123 Povo, Trento, Italy
*marc.eisenmann@nao.ac.jp

Received 18 March 2024; revised 25 April 2024; accepted 25 April 2024; posted 26 April 2024; published 7 June 2024

GW detectors are ultimately limited by thermal noise in their most sensitive region. Cryogenic operation combined with crystalline substrates and coatings is a promising approach to reduce this noise, thereby increasing their sensitivity and detection rate. However, crystalline materials can exhibit birefringent behaviors which will degrade the detector's sensitivity. Here, we demonstrate the use of a pair of identical electropolarization retarders to generate arbitrary polarization states and compensate birefringence of a KAGRA test-mass substrate.

https://doi.org/10.1364/OL.523753

Introduction. Since the first direct detection of gravitational waves (GW) in 2015 [1], the GW detection rate has drastically increased from about once a month to few per week [2]. This increase is due to the improvement in the detector's sensitivity. Detectors are limited in their most sensitivity frequency band by the test-masses' coating thermal noise [3]. KAGRA [4] and future GW detectors (such as Voyager [5], a possible upgrade plan of the Advanced LIGO detectors [6] or the Einstein Telescope [7]) will operate with test-masses at cryogenic temperature. Cryogenic operation will reduce thermal noise and consequently increase the detection rate. These detectors rely on crystalline substrates (such as sapphire or silicon) for their high optical and mechanical properties at cryogenic temperature. Additionally, crystalline coatings are promising candidates to reduce the coating Brownian noise [8].

However, such crystalline materials exhibit birefringence [8–10]. Uniform static birefringence, either inherent to the material or induced by a stress or thermal effect, is a source of depolarization that will spoil the interferometer contrast [11]. The test-masses' substrate of the KAGRA detector exhibits non-uniform static birefringence [12] that is responsible for the non-uniform distortion of the transmitted wavefront error maps. Such distortion is causing degradation of the shot noise, higher coupling to the laser noise, and coupling to alignment control signals that spoil KAGRA sensitivity [13,14]. The presence of birefringence noise was reported for crystalline coatings [15] that could become a limiting noise source [16]. This birefringence noise could also limit the sensitivity of axion dark matter search based on the axion-photon coupling inside optical cavities [17–19].

While smaller samples can exhibit low birefringence, the complexity in the growth of large crystals makes the extension of measurements from smaller to larger samples non-trivial. Currently, large dimension (40–200 kg, 30–55 cm in diameter) crystalline substrates and coatings required for future upgrades of the detectors, are not being manufactured and characterized. This makes it possible for large crystals to exhibit birefringence.

In this Letter, we propose and demonstrate for the first time to our knowledge a method to compensate for birefringence. It is based on a pair of identical electronically tunable polarization retarders that can generate arbitrary polarization states. This enables birefringence compensation by modifying the input polarization incident on a birefringent material so to recover the wanted polarization in its transmission or reflection. Such components could be used to compensate for the birefringence coupling to control signals of GW detectors where only modest requirements in optical losses and low optical power are used. This technique also opens the door for possible birefringence compensation of the main laser beam circulating within the GW detector. It should be noted that both the Advanced LIGO and Virgo detectors are already using thermal compensation systems for the main beam circulating inside the detectors to compensate for the non-uniform wavefront distortion induced by optical absorption inside the test-masses [20,21]. With appropriate R&D, it could be possible to adapt these systems for birefringence compensation. Indeed, the method presented in this Letter relies on the use of identical variable polarization retarders. This drastically eases the required search for a suitable material that can offer the capabilities of birefringence compensation as only a single suitable material to be used in pair is required. Furthermore, such technique can also be used to directly measure samples' birefringence.

A pair of liquid crystal cells as a polarization state generator. Full control of a polarization state generally requires the use of two actuators, thereby offering control of retardation and rotation of the polarization. For instance, one of the KAGRA's birefringence characterization experiment uses a Soleil–Babinet compensator and a rotating half-wave plate (HWP) in order to perform a direct birefringence measurement [22]. They act on the polarization retardation and rotation angle, respectively. However, it requires to probe a large parameter space with mechanical actuators, making the measurement slow (about 0.03 Hz). To reduce the characterization time, we propose to use instead a pair of electro-optic components, here a liquid crystal (LC), and directly control the polarization state at drastically higher speed. LCs are birefringent molecules that align with the applied electrical field. Since their discovery in 1888 [23], they attracted scientific interest with the manufacturing of the LC with the largest birefringence among known materials [24]. But it is mainly through the invention of the liquid crystal display (LCD) technology that LC use developed. For our purpose, we use LCs as they are able to generate large retardation at several tens of Hz while only requiring low voltages. In addition, they present the advantage to be scaled as a 2D array, thereby opening the window for 2D polarization control and characterization.

The evolution of the polarization states can be described using the Jones formalism [25]. The Jones matrix of a variable retarder $T(\theta, \epsilon(V))$ can be expressed as

$$T(\theta, \epsilon(V)) = \begin{pmatrix} \cos\theta & -\sin\theta \\ \sin\theta & \cos\theta \end{pmatrix} \begin{pmatrix} e^{\frac{i\epsilon(V)}{2}} & 0 \\ 0 & e^{\frac{-i\epsilon(V)}{2}} \end{pmatrix} \begin{pmatrix} \cos\theta & \sin\theta \\ -\sin\theta & \cos\theta \end{pmatrix}, \tag{1}$$

where θ and $\epsilon(V)$ are the component fast-axis angle with respect to the input polarization direction and its voltage-dependent retardation, respectively. Using Eq. (1), the effect of a pair of variable polarization retarders on an input linear polarization can be described as in Eq. (2). In that case, the first LC fast axis is oriented at 45° of the input polarization direction, and the second LC fast axis is aligned with the input polarization and the output polarization state described by its Jones vector J_{out} is only dependent on the voltage applied to each LC:

$$J_{out} = T(0, \epsilon(V_2)) \cdot T(45, \epsilon(V_1)) \cdot \begin{pmatrix} 1 \\ 0 \end{pmatrix} = \begin{pmatrix} \cos\dfrac{\epsilon(V_1)}{2} \cdot e^{+i\frac{\epsilon(V_2)}{2}} \\ i\sin\dfrac{\epsilon(V1)}{2} \cdot e^{-i\frac{\epsilon(V_2)}{2}} \end{pmatrix}. \tag{2}$$

It shows that the polarization state transmitted by this pair of variable polarization retarder is arbitrary with the polarization rotation and retardation controlled respectively by the first and second retarders.

Liquid crystal calibration. For arbitrary polarization state generation, it is first required to characterize the LC. This includes evaluating its voltage-induced retardation and fast-axis alignment with respect to the input polarization direction. In this experiment, we use a pair of temperature-controlled LC cells (LCC1111T-C, Thorlabs) along with a polarization camera in the readout part (PAX-1000-IR2, Thorlabs). The polarization camera has a resolution for polarization rotation or azimuth angle of ±0.03° and retardance of ±0.04°. The input polarization was tuned to reach azimuth and ellipticity angles down to the polarization camera resolution by tuning the quarter-wave plate (QWP) and HWP placed before the LC. They allow to compensate the possible birefringence of the beam splitter. The beam splitter reflection is monitored by a photodiode which is used to normalize the power transmitted by the output polarizer and therefore minimize the effects of laser power fluctuations. In this experiment, the input laser power is set to about 12 mW and the beam size on the LC and the sample is about 1 mm in diameter.

The LC characterization setup is presented in Fig. 1 where the LCs are installed between two Glan–Taylor polarizers with an extinction ratio of about 100,000 used in the cross-polarizer configuration.

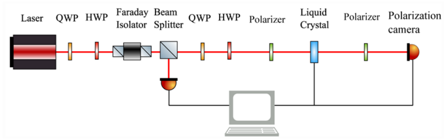

Fig. 1. Experimental setup used to characterize each liquid crystal. The two polarizers are installed in cross-polarizer configuration.

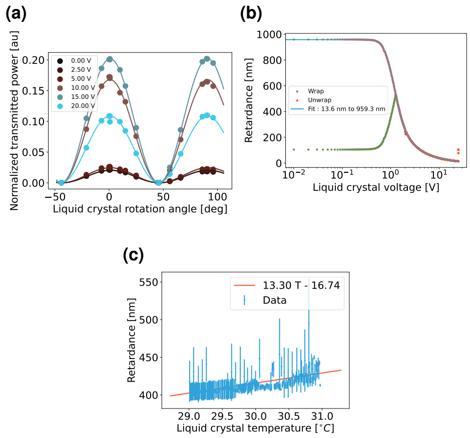

Fig. 2. Characterization of liquid crystal cell. (a) Transmitted power as a function of the liquid crystal rotation. Liquid crystal retardance as a function of (b) applied voltage and (c) temperature.

The input power is used to normalize the transmitted power to minimize the effects of laser power fluctuations. The LC's fast axis can be identified by rotating it and monitoring the normalized transmitted power. Indeed, this configuration can be described in the Jones formalism by the transmitted Jones vector J_{tra}:

$$J_{tra} = \begin{pmatrix} 0 & 0 \\ 0 & 1 \end{pmatrix} \cdot T(\theta, \epsilon(V)) \cdot \begin{pmatrix} 1 \\ 0 \end{pmatrix} = \begin{pmatrix} 0 \\ 2\cos(\theta)\sin(\theta)\cos\left(\dfrac{\epsilon(V)}{2}\right) \end{pmatrix}. \tag{3}$$

The normalized transmitted power $P(\theta)$ can be computed from Eq. (3) as

$$P(\theta) = \left(2\cos(\theta)\sin(\theta)\cos\left(\frac{\epsilon(V)}{2}\right)\right)^2 = \cos^2\left(\frac{\epsilon(V)}{2}\right)\sin(2(\theta))^2, \tag{4}$$

where $\theta = \theta_{rot} - \theta_0$ with θ_{rot} and θ_0 the LC's rotation angle and θ_0 an arbitrary offset angle when installing the LC inside its rotator mount. The maximal and minimal power is obtained when the LC's fast axis is at $\theta = 45°$ and $\theta = 0°$ of the input polarization direction, respectively.

The LC was rotated using a motorized mount (PRM1, Thorlabs) and for each rotation, the LC voltage was scanned from 0 to 25 V. Parts of the results are presented in Fig. 2(a) where the horizontal axis represents $\theta_{rot} = \theta - \theta_0$. This measurement allowed us to identify the LC's fast-axis angle and confirm that its orientation is independent from the voltage applied to the LC. Furthermore, it is possible to estimate the misalignment of the LC's fast axis with respect to the input polarization direction (using Eq. (1)) which is 0.1°, at the resolution level of the motorized rotator.

Using the measurement with the LC's fast axis at 45° from the input polarization, it is possible to measure the LC retardation as a function of the applied voltage. The retardation (in nm) R^{nm} can be computed from the transmitted power P using

$$R^{nm} = 2\arcsin\sqrt{P}\frac{\lambda}{2\pi},$$

where λ is the laser wavelength. As the LC is generating more than half-wave retardation, it is required to unwrap the reconstructed retardation. The LC used in this experiment is uncompensated: at high voltage, it induces a small positive retardation. As we expect the maximal retardation to be at minimum voltage, the unwrapping is done by flipping all retardation over the maximum unwrapped retardation at low voltages. The reconstructed retardation is shown in Fig. 2(b) and varies between about 14 to 959 nm which is in agreement with the manufacturer's calibration data. The measurement presented in this figure is the mean of 10 voltage scans. Using this equation, it is also possible to estimate the effect of the cross-polarizers on the estimated retardation from the normalized transmitted power without the LC installed. We measured $P = 3.97 \cdot 10^{-6}$ giving $R^{nm} = 0.67$ nm.

Here, the LC control and photodiode data acquisition are automatized using a Labview. Due to the switch speed of the LC, the voltage and therefore the retardance control are limited to 80 Hz.

Because the temperature of a LC cell affects its retardance [26,27], it is required to implement temperature control to ensure the long-term stability of the LC's performances. We measured the effects of temperature on the LC retardance by varying the LC temperature around its set point while maintaining its voltage at 0 V. This measurement is shown in Fig. 2(c) where the wrapped retardance is plotted as a function of the LC's temperature. The wrapped retardance is changing as 13.1 nm/$^\circ C$ which means that the effective (or unwrapped) retardance is changing by -13.1 nm/$^\circ C$. A temperature control with PID was implemented to ensure that each LC temperature is stabilized to $(30 \pm 0.1)^\circ$C. With the implemented temperature control, the temperature effects on the retardation are reduced to 1.3 nm fluctuations. All previous characterization measurements were performed with controlled temperature.

Arbitrary polarization state generation. As described previously, it is possible to generate arbitrary polarization states with a pair of LCs properly aligned with respect to the input polarization. They are installed such that LC1's and LC2's fast axis are at 45° and 0° of the input polarization direction, respectively. Each LC's temperature is controlled within ±0.1°C.

The voltages applied to each LC are scanned from 0 to 25 V with 10 mV step. The light transmitted by the pair of LCs is then acquired by the polarization camera. The generated polarization states are presented in Fig. 3. The expected behavior is visible: LC1 (LC2) mainly acts on the azimuth (ellipticity) angle as in Figs. 3(a) and 3(b). Furthermore, about 6.3 million polarization states are generated at 40 Hz which cover most of the polarization states' parameter space as shown in Fig. 3(c). The operation speed of a pair of LCs is reduced by a factor 2 compared to the operation speed of a single one. The speed should be recovered by further optimizing the Labview program. However, this polarization state generation is already an order of magnitude faster than the previous birefringence characterization experiments in the KAGRA collaboration [9,22]. The ellipticity angles vary from -90 to $+90°$ and azimuth angles from -45 to $+45°$. The number of generated polarization states was limited by measurement duration, but using 1 mV (voltage controller resolution) instead of 10 mV can generate 100 times more polarization states.

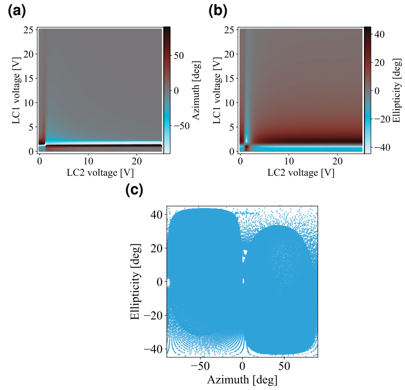

Fig. 3. Polarization states generation using a pair of liquid crystal cells. (a) Polarization azimuth and ellipticity (b) as a function of the applied voltage. (c) Generated polarization states ellipticity as a function of azimuth.

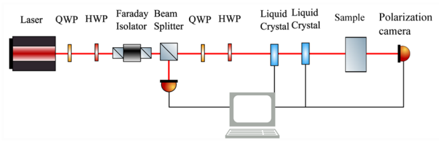

Fig. 4. Experimental setup used to compensate birefringence of a substrate.

This demonstrates that a pair of LCs or any electro-optic crystals can be used as an electronically driven polarization state generator. This device can then be operated as a fast birefringence measurement device, drastically decreasing the measurement duration of the KAGRA test-mass substrate birefringence [9,22]. Another possible use of this device can be to compensate the sample's birefringence by modifying the input polarization so to recover the input polarization state after the sample.

Birefringence compensation. The test-masses of the KAGRA detector are made of 23 kg sapphire substrates. To achieve cryogenic temperature while using high laser power circulating through the input test-mass substrate, it is required that the sapphire substrates have optical absorption of less than 50 ppm/cm [4]. For that purpose, we developed an absorption mapping apparatus that can measure optical absorption with sub-ppm resolution for a sample from 1.27 to 22 cm in diameter [28]. Following the rediscovery of the birefringence issue for the KAGRA detector [13,14], this characterization setup has been modified to be able to measure birefringence maps. We were able to characterize a sapphire substrate that was a candidate test-mass for KAGRA and exhibited birefringence of about $\Delta n \sim 10^{-6}$ and $\theta \sim 1 - 10°$ with fluctuations of similar magnitude over its entire surface [9].

For our purpose, we installed this pre-characterized sample between the pair of LCs and the polarization camera as in Fig. 4.

We scanned the voltages of each LC between 0 and 25 V with a 0.1 V increment and simultaneously monitored the transmitted retardance and azimuth angles. This measurement is repeated with the LCs' voltages close to the minimal absolute values of retardance and azimuth angles with finer step size, up to 1 mV. In order to compare this result with the previous measurement, the resulting ellipticity measured in deg R° can be converted into

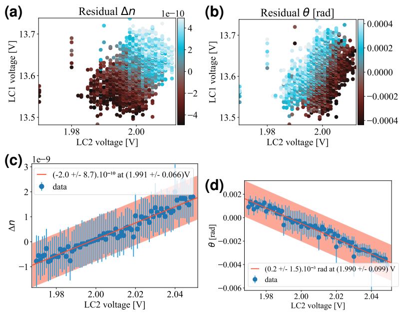

Fig. 5. Birefringence compensation of a 23 kg saphire substrate with a pair of liquid crystal cells. (a) Residual Δn and (b) θ for voltages that minimize them both. (c) Residual Δn and (d) θ fixing the first liquid crystal voltage to 13.59 V.

Δn by using

$$\Delta n = \frac{R^{\circ}}{360}\frac{\lambda}{d}, \tag{5}$$

where $\lambda = 1064$ nm is the laser wavelength and $d = 15$ cm is the sample's thickness.

Finally, we keep the data for which the absolute values of retardance and azimuth angles are both below 0.025°. The resulting data corresponds to the generation of polarization states by the pair of LCs that compensate the sample birefringence within ±0.025°. The corresponding measurement is presented in Figs. 5(a) and 5(b) for the obtained residual Δn and θ, respectively.

Equation (5) can also be used to estimate the uncertainty on these measurements. In Figs. 5(c) and 5(d), the residual Δn and θ are plotted, respectively.

For these figures, the LC1 voltage is kept constant to 13.59 V, while the LC2 voltage is varied between 1.96 and 2.06 V. These values were chosen so that both residual Δn and θ reached their minimum absolute value for identical voltages applied to the pair of LCs. The data in blue represents measurements with associated error bar from the polarization camera uncertainty, whereas the red line depicts a linear fit of the data and the red area represents the 1σ fitting error. The fit gives a residual Δn of $(-2 \pm 8.7) \cdot 10^{-10}$ and residual θ of $(0.2 \pm 1.5) \cdot 10^{-3}$ rad.

It can be seen from the residual values that the rather large uncertainty is dominated by the polarization camera error. On the other hand, the LC actuation is limited by its voltage driver resolution (1 mV). From the fitted slope, it is possible to extract the actuation of the pair of LCs on both Δn and θ to be $(3.25 \pm 0.09) \cdot 10^{-8}$ /V and $(-6.55 \pm 0.15) \cdot 10^{-2}$ rad/V. It means that the smallest achievable birefringence actuation is $\Delta n_{min} = (3.25 \pm 0.09) \cdot 10^{-11}$ and $\theta_{min} = (-6.55 \pm 0.15) \cdot 10^{-5}$ rad.

As shown in Fig. 3, the pair of LCs is able to cover most of the polarization states' space parameters. It means that it is able to compensate the birefringence of the KAGRA size sample down to Δn_{min} and θ_{min}. This corresponds to a reduction of both Δn and θ by a factor of 10^5.

Conclusion. In this Letter, we demonstrate the use of a pair of electronic polarization variable retarders to generate arbitrary polarization states. It is especially possible to modify the input polarization state and compensate a sample's birefringence by a factor of 10^5. While LCs manifest too much losses (about 98 % transmission measured) to be used for the main beam of GW detectors, they could be used to compensate for birefringence effects on control beams with less stringent requirements on optical losses, power density, and wavefront distortion. If lower optical losses and higher power density are required, different materials (for instance, electro-optic crystals [29]) could also be used. This method also opens the possibility to compensate for the birefringence of optical beams with more stringent requirements, such as the main beam of GW detectors. It is required to develop a single polarization variable retarder with appropriate properties. Its use in a pair would then provide full polarization control and therefore achieve birefringence compensation. This will be the target of future studies. Furthermore, it will allow to develop faster birefringence characterization which is mandatory for the next generation of GW detectors.

Funding. Ministry of Education, Culture, Sports, Science and Technology (220003); Japan Society for the Promotion of Science (20F20803, 23K19053).

Disclosures. The authors declare no conflicts of interest.

Data availability. Data underlying the results presented in this paper are not publicly available at this time but may be obtained from the authors upon reasonable request.

REFERENCES

1. B. P. Abbott, R. Abbott, T. D. Abbott, *et al.*, Phys. Rev. Lett. **116**, 061102 (2016).
2. R. Abbott, T. D. Abbott, F. Acernese, *et al.*, Phys. Rev. X **13**, 041039 (2023).
3. Y. Levin, Phys. Rev. D **57**, 659 (1998).
4. T. Akutsu, M. Ando, K. Arai, *et al.*, Prog. Theor. Exp. Phys. **2021**, 05A101 (2020).
5. R. X. Adhikari, K. Arai, A. F. Brooks, *et al.*, Classical Quantum Gravity **37**, 165003 (2020).
6. T. L. S. Collaboration, J. Aasi, B. P. Abbott, *et al.*, Classical Quantum Gravity **32**, 074001 (2015).
7. M. Punturo, M. Abernathy, F. Acernese, *et al.*, Classical Quantum Gravity **27**, 194002 (2010).
8. G. Cole, W. Zhang, M. Martin, *et al.*, Nat. Photonics **7**, 644 (2013).
9. S. Zeidler, M. Eisenmann, P. Li, *et al.*, Sci. Rep. **13**, 21393 (2023).
10. C. Krüger, D. Heinert, A. Khalaidovski, *et al.*, Classical Quantum Gravity **33**, 015012 (2015).
11. W. Winkler, A. Rüdiger, R. Schilling, *et al.*, Opt. Commun. **112**, 245 (1994).
12. H. Wang, Y. Aso, M. Leonardi, *et al.*, "Characterization of birefringence inhomogeneity of kagra sapphire mirrors from transmitted wavefront error measurements," arXiv, arXiv: 2402.18006v1(2024).
13. K. Somiya, E. Hirose, and Y. Michimura, Phys. Rev. D **100**, 082005 (2019).
14. C. Kagra, Prog. Theor. Exp. Phys. **2023**, 10A101 (2022).
15. J. Yu, S. Häfner, T. Legero, *et al.*, Phys. Rev. X **13**, 041002 (2023).
16. Y. Michimura, H. Wang, F. Salces-Carcoba, *et al.*, Phys. Rev. D **109**, 022009 (2024).
17. I. Obata, T. Fujita, and Y. Michimura, Phys. Rev. Lett. **121**, 161301 (2018).
18. D. Martynov and H. Miao, Phys. Rev. D **101**, 095034 (2020).
19. K. Nagano, H. Nakatsuka, S. Morisaki, *et al.*, Phys. Rev. D **104**, 062008 (2021).
20. A. F. Brooks, B. Abbott, M. A. Arain, *et al.*, Appl. Opt. **55**, 8256 (2016).
21. T. Accadia, F. Acernese, F. Antonucci, *et al.*, in *Marcel Grossman Meeting on General Relativity* (World Scientific, 2012), pp. 1652–1656.
22. M. Tokunari, H. Hayakawa, K. Yamamoto, *et al.*, J. Phys.: Conf. Ser. **32**, 432 (2006).
23. F. Reinitzer, Liq. Cryst. **5**, 7 (1989).
24. J. Zadoc-Kahn, Nature **123**, 113 (1929).
25. R. C. Jones, J. Opt. Soc. Am. **31**, 500 (1941).
26. I. Haller, Prog. Solid State Chem. **10**, 103 (1975).
27. P. G. Parejo and A. Álvarez Herrero, Opt. Mater. Express **9**, 2681 (2019).
28. M. Marchio, M. Leonardi, M. Bazzan, *et al.*, Sci. Rep. **11**, 2654 (2021).
29. J. Kaneshiro, T. M. Watanabe, H. Fujita, *et al.*, Appl. Opt. **55**, 1082 (2016).